Shape-Engineered multifunctional porous silicon nanoparticles by direct imprinting

2015 Nanotechnology 26 271001

(http://iopscience.iop.org/0957-4484/26/27/271001)

Fast Track Communications

IOP Publishing Nanotechnology

Nanotechnology **26** (2015) 271001 (8pp) doi:10.1088/0957-4484/26/27/271001

Fast Track Communication

Shape-Engineered multifunctional porous silicon nanoparticles by direct imprinting

Jeremy W Mares[1], Joshua S Fain[1], Kelsey R Beavers[2], Craig L Duvall[3] and Sharon M Weiss[1]

[1] Department of Electrical Engineering and Computer Science, Vanderbilt University, Nashville, TN 37235, USA
[2] Interdisciplinary Graduate Program in Materials Science, Vanderbilt University, Nashville, TN 37235, USA
[3] Department of Biomedical Engineering, Vanderbilt University, Nashville, TN 37235, USA

E-mail: sharon.weiss@Vanderbilt.edu

Received 24 April 2015, revised 12 May 2015
Accepted for publication 19 May 2015
Published 17 June 2015

Abstract

A versatile and scalable method for fabricating shape-engineered nano- and micrometer scale particles from mesoporous silicon (PSi) thin films is presented. This approach, based on the direct imprinting of porous substrates (DIPS) technique, facilitates the generation of particles with arbitrary shape, ranging in minimum dimension from approximately 100 nm to several micrometers, by carrying out high-pressure (>200 MPa) direct imprintation, followed by electrochemical etching of a sub-surface perforation layer and ultrasonication. PSi particles (PSPs) with a variety of geometries have been produced in quantities sufficient for biomedical applications ($\gg$10 μg). Because the stamps can be reused over 150 times, this process is substantially more economical and efficient than the use of electron beam lithography and reactive ion etching for the fabrication of nanometer-scale PSPs directly. The versatility of this fabrication method is demonstrated by loading the DIPS-imprinted PSPs with a therapeutic peptide nucleic acid drug molecule, and by vapor deposition of an Au coating to facilitate the use of PSPs as a photothermal contrast agent.

Keywords: thin films, nanomedicine, porous silicon, drug delivery, nanofabrication

(Some figures may appear in colour only in the online journal)

1. Introduction

Drug delivery research has established that particle shape and size significantly influence biodistribution of nanoparticle therapeutic delivery vehicles as well as the route and degree of particle internalization by cells [12, 16, 17, 23, 32, 46]. Passive cell targeting, hemodynamic-dependent vascular distribution, drug release rates, and responsiveness to external stimulus are all examples of functions that can be realized in part by controlling the geometry of the drug delivery vehicle [1, 10, 12–14, 17, 22, 37, 46]. A number of promising material platforms have been investigated as candidates for shape-engineered nano- or microparticles. These include polymeric particles such as solvent-molded polystyrene and poly(vinyl alcohol) [9], lithographically-fabricated polyethylene glycol diacrylate [14], and other soluble or melt-processable polymers fabricated by a particle replication in nonwetting templates processes [26]. In addition, inorganic particles that have been shape-engineered include fullerenes [4], metallic nanoparticles [36], and silica nanoparticles [41] which are most often fabricated by bottom-up, solution-phase synthesis.

A promising emergent candidate material for targeted drug delivery is PSi [2, 3, 7, 25, 34, 44]. This nanostructured material is fabricated most commonly through electrochemical etching of single crystal Si and is characterized by

densely-packed and well-aligned nanometer scale pores that impart to the material an exceptionally large internal surface area ($\gg$100 $m^2\,cm^{-3}$) [6, 11, 20, 38]. PSi has a good cytotoxicity profile [2, 7, 35, 39], exhibits good stability in the biological environment, and has a tunable degradation rate based on its degree of oxidation. PSi can also support a variety of chemical surface functionalization and attachment chemistries [2, 3, 21, 24], and its porosity and degradation characteristics can be exploited to facilitate the sustained release of drug molecules [10, 25, 40, 44]. For these reasons, PSi drug delivery has been investigated over the past several years for targeted delivery of therapeutic small molecules as well as oligomers [2, 34, 42, 44].

PSi particles (PSPs) have been traditionally fabricated by fracturing PSi films through processes such as ball milling and ultrasonic fragmentation [5, 25, 34, 35, 44]. Such methods, while effective for producing large quantities of particles, yield particles that are irregular in shape or tending towards spherical, and generally polydisperse. Moreover, in the case of ball milling, contamination is often an issue. Recently, more refined methods for the fabrication of particles from PSi have been developed, opening up the potential for this material to be utilized in advanced biomedical applications [10, 31]. Using UV lithography and reactive ion etching (RIE) techniques, shape-engineered PSPs that are several micrometers in size have been fabricated in medically relevant quantities for the staged-release of drug molecules (i.e., > tens of μg for *in vitro* work and mg quantities for *in vivo* studies [25]), facilitating multi-vector design of PSi drug delivery vehicles [10, 15, 40]. However, using this approach, it is very challenging to fabricate particles with feature sizes significantly below the wavelength of UV light employed in the patterning step (typically ~400 nm). In contrast, patterning by electron beam lithography (EBL) can write particle features <100 nm but the process is extremely time-inefficient and economically prohibitive. For example, patterning a 1 mm^2 region of nanometer-scale features by EBL with a high density of features (i.e., a fill factor >50%) requires more than 1 h. For PSi films of 200 nm thickness and 70% porosity, this would yield approximately 140 ng of shape-engineered particles. However, even a simple *in vitro* experiment generally requires at least 100 times that mass of nanoparticles, making patterning by direct EBL writing an impractical option.

A promising approach to overcoming this limit in yield for submicron PSPs is to employ a reusable stamp as a means to pattern nanoparticles directly into PSi thin films. Stamp and mold-based patterning processes have been successfully used to shape-engineer polymeric nanoparticles for biomedical applications [26]. Patterning more rigid mesoporous thin films by imprintation, however, presents unique challenges due to the significantly greater forces required for pattern transfer. Ryckman *et al* established such a method for patterning porous thin films and termed the process the direct imprinting of porous substrates (DIPS) [31]. DIPS has been applied to pattern PSi, nanoporous Au, titania nanotubes and other materials with feature sizes below 100 nm, and the process has been utilized to fabricate a variety of on-substrate structures including diffraction-based biosensors, surface-enhanced Raman spectroscopy substrates, and three-dimensionally patterned surface structures from porous films [18, 29, 30].

Here, we report on advancements in the DIPS process that enable the fabrication of medically relevant quantities of shape-engineering PSPs. The shape of the PSPs is determined entirely by the shape defined on the stamp used to pattern the particles and is therefore not limited to only disks and rods. We present a refined means of detaching DIPS-patterned particles from the PSi substrate that minimizes PSi debris by use of an optimized high porosity perforation layer following imprintation. We also demonstrate drug-loading of these particles with therapeutic peptide nucleic acid (PNA) molecules, and functionalization by thermal deposition of Au to impart photothermal properties to the particles. A well-characterized anti-microRNA PNA molecule whose suppression has been linked to decreased hepatitis C viremia, anti-miR122 (NH_2-ACA AAC ACC ATT GTC ACA CTC CA-cys-COOH), was selected as the model therapeutic PNA [19, 28]. This work demonstrates that direct imprintation is a viable approach for fabrication of multifunctional, shape-engineered PSi nanoparticles in quantities sufficient for the pre-clinical testing of PSi therapeutics.

2. Experimental section

2.1. DIPS process for particle fabrication

The DIPS process for particle fabrication is illustrated in figure 1(a). PSi thin films were first electrochemically etched from highly-doped p-type Si substrates (0.01 Ω cm) with a solution of 15% hydrofluoric acid in ethanol to form single layers of PSi, approximately 250 nm in thickness and 2 cm^2 in area [33]. Etch current densities ranging from 50 to 70 mA cm^{-2} were applied to form PSi films with porosities ranging from approximately 76 to 84%. Separately, relief structure stamps were fabricated from single-crystal Si using either conventional UV lithography for micrometer-scale PSPs or EBL for smaller particles (<2 μm), followed by RIE to yield stamps with features of 250 nm depth. In general, stamps of any size may be fabricated, limited only by the resolution of the lithographic approach and the thickness of the starting wafer. In this work, we chose a stamp size of approximately 2×2 mm^2. The low aspect ratio of the stamps reduces the probability of mechanical fracture upon multiple imprintations. In order to prevent adhesion of PSi to the stamps during imprintation, both the stamp and the PSi film are surface-functionalized with trichloro (1H,1H,2H,2H-perfluorooctyl) silane (97%, Signma-Aldrich). Treatment with the silane is carried out by placing the stamp and PSi film in a vacuum desiccator with 100 μL of the silane in an open vial. The chamber is then held under weak vacuum for >2 h allowing for the vapor-phase attachment of the silane to the Si surfaces. Treating both the stamp and the film with the silane results in minimal adhesion of PSi to the stamp. For biomedical applications in which residual silane on the PSPs could introduce adverse biological effects, simply silane-

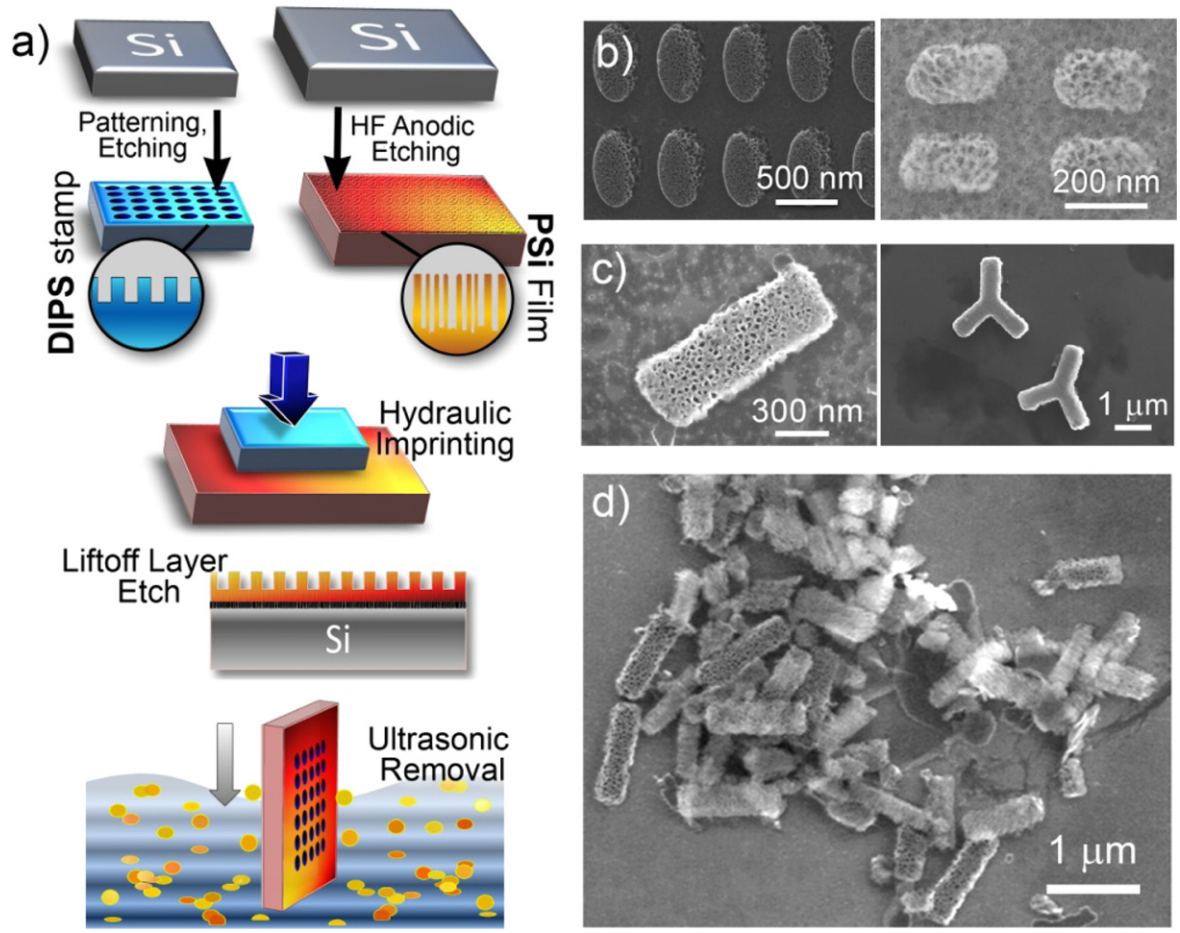

Figure 1. (a) Process flow for DIPS particle fabrication, (b) elliptical and rectangular nanoparticles on substrate, prior to removal by ultrasonication, (c) rectangular and y-shaped particles after ultrasonic removal from the substrate, and (d) an agglomerate of PSPs, aspect ratio = 4, showing good uniformity with minimal interstitial debris.

functionalizing the stamp is a viable option since the additional silane treatment of the PSi film leads to only a modest further reduction in PSi adhesion. Alternatively, if both the film and stamp are silanized, the silane may be removed from the particles following fabrication by treatment with sulfuric acid and subsequent thorough rinsing with water or other solvents.

Following stamp and PSi film preparation, the DIPS process is carried out using a hydraulic ring press (RIIC) equipped with a calibrated pressure gauge (Winters Instruments), as shown in figure 2(a). Polished steel press plates provide flat surfaces for contact with the PSi film and stamp. The lower press plate is equipped with four height-adjustable spring-loaded plunger pins, located approximately 7 cm from the stamp, which help to facilitate uniform imprintation across the imprinted region. A pair of beveled washers located between the top press plate and the press' thrust bearing ensure that the direction of applied force is perpendicular to the plane of the PSi film. Pressure, ranging from 200 to 400 MPa is applied to yield uniformly imprinted features, as shown in figure 2(b). A single imprintation can be carried out in 1–2 min. Because the stamp footprint used in this work is significantly smaller than that of the PSi film, multiple imprintations on the same PSi film are performed. The depth of the stamp features are greater than or equal to the thickness of the PSi film, such that PSi regions between the desired particle features are crushed and mechanically compacted, leaving the particle regions uncompressed.

After pattern imprintation, the PSPs are still attached to the surface of the Si substrate, which is in contrast to some imprintation methods in which imprinted particles adhere to the mold itself following imprinting. To facilitate the removal of the particles from the substrate, a second, sacrificial PSi layer with very high porosity layer (approaching 100%, referred to herein as a perforation layer) is then etched by applying an etch current density of 270 mA cm^{-2} for a duration of 3.25 s to facilitate PSP removal from the substrate, similar to the release layer used by Godin *et al* [15]. This second electrochemical etching step does not affect the imprinted particles as the etch front begins at the pore tips at the bases of the particles and crushed regions [31, 33]. Following the perforation layer formation, the PSi film (with particles still attached) is carefully rinsed with ethanol and dried with N_2. The substrate to which the particles are attached is then ultrasonicated briefly (5–60 s) to remove the particles from the Si substrate into suspension (figure 2(c)). Commonly, isopropyl alcohol was used as the suspending medium. It is important to note that the efficiency with which

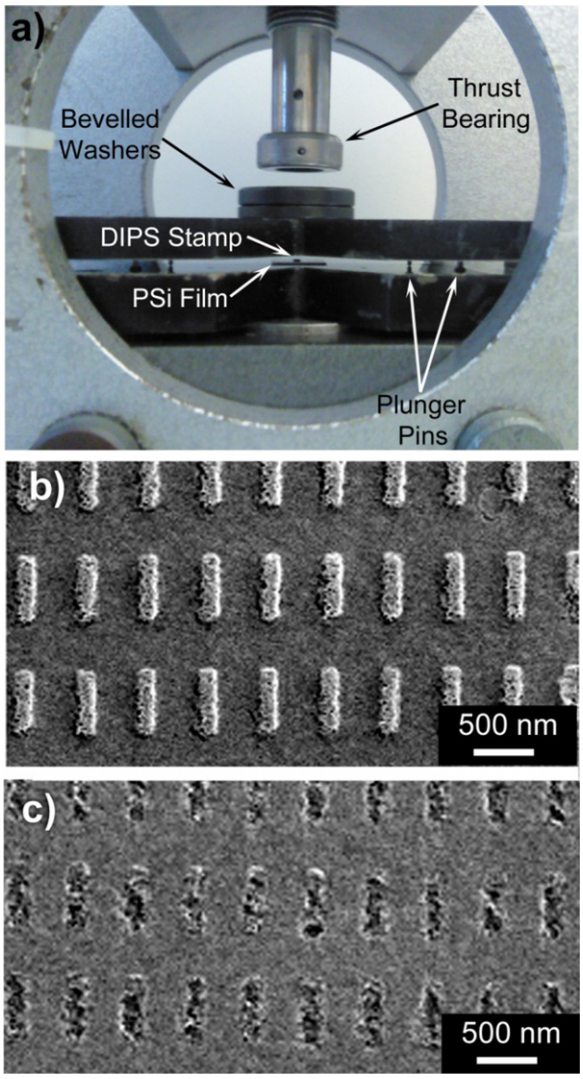

Figure 2. (a) The hydraulic ring press employed for PSi imprintation, (b) PSi nanoparticles (150×600 nm^2) on substrate following imprintation and (c) imprinted PSi substrate following particle removal by ultrasonication.

PSPs are removed from the substrate is highly sensitive to variations in the etch current density used for the perforation layer. If the etch current density is too small, it precludes effective subsequent removal from the substrate. If the current density or etch time are too large, the particles may detach from the substrate during etching of the perforation layer, making recovery impractical, and the imprinted, interstitial region between particles may detach during ultrasonication along with the desired particles, contributing to an unacceptable content of irregularly-shaped debris. Refinement of the etch parameters to realize this perforation layer therefore represents a significant milestone in the DIPS process.

2.2. Characterization of pattern transfer

In order to quantify degree of imprintation as a function of applied pressure, the percent of total stamp area patterned on the PSi film for a range of applied pressures was measured. This metric, which gives an indication of the appropriate pressure range for uniform pattern transfer, is simpler to quantify than depth of imprintation versus pressure because imprintation depth can be non-uniform across the stamp region for pressures below the minimum required for complete pattern transfer. This is because perfect uniformity and perpendicularity of imprintation force is not possible using conventional instrumentation, and elastic stamp deformation also occurs, resulting in regions of imprintation that vary in depth. At pressures greater than the minimum pressure required for uniformity, however, further elastic deformation of the stamp ensures that the entire imprinted region is uniform in depth. After carrying out imprinting, optical microscopy is used to image the imprinted region, and image analysis software (ImageJ) is employed to quantify the fraction of total possible stamp area that is transferred to the PSi film. This quantification of the imprinted region is made possible by the color change that is induced when a region of PSi is compressed. This is illustrated in figure 3(a), which shows an 80% porosity PSi film after imprintation with 193, 238 and 314 MPa of pressure. In these images, the imprinted, compacted region is on the left side of each micrograph, and the patterned area clearly grows with increasing imprintation force. This optical method, while unable to resolve individual particles, is therefore an effective means of quantifying fractional imprintation for a printed area of PSi.

2.3. PSP functionalization

To demonstrate internal surface functionalization of PSPs fabricated by our DIPS process, anti-miR122 PNA was loaded into the PSPs by first immersing them in a solution of PNA dissolved in 50% ethanol and water for 4 h. Particles were then pelleted by centrifugation and supernatant containing free PNA was removed. The pellet was then dried by lyophilization to impregnate the particles with PNA. Physically absorbed PNA was cross-linked within the particles using succinimidyl 3-(2-pyridyldithio)propionate (SPDP) to reduce free diffusion of drug from the pores. External surface functionalization of DIPS-fabricated PSPs was demonstrated by using a resistive evaporator (Angstrom Engineering) to deposit 40 nm Au onto imprinted PSPs on-chip, following etching of the perforation layer but before ultrasonication.

2.4. PSP characterization

The mass of PSPs in suspension was quantified by inductively-coupled plasma optical emission spectroscopy (ICP-OES, Varian ICP model 720-ES). The morphology and composition of the bare and functionalized PSPs were characterized by scanning electron microscopy (SEM, Hitachi-S4200 and Raith eLine) along with transmission electron microscopy (TEM) and energy dispersive x-ray spectroscopy (EDS) mapping using an FEI Tecnai Osiris transmission/scanning transmission microscope operated at 200 keV.

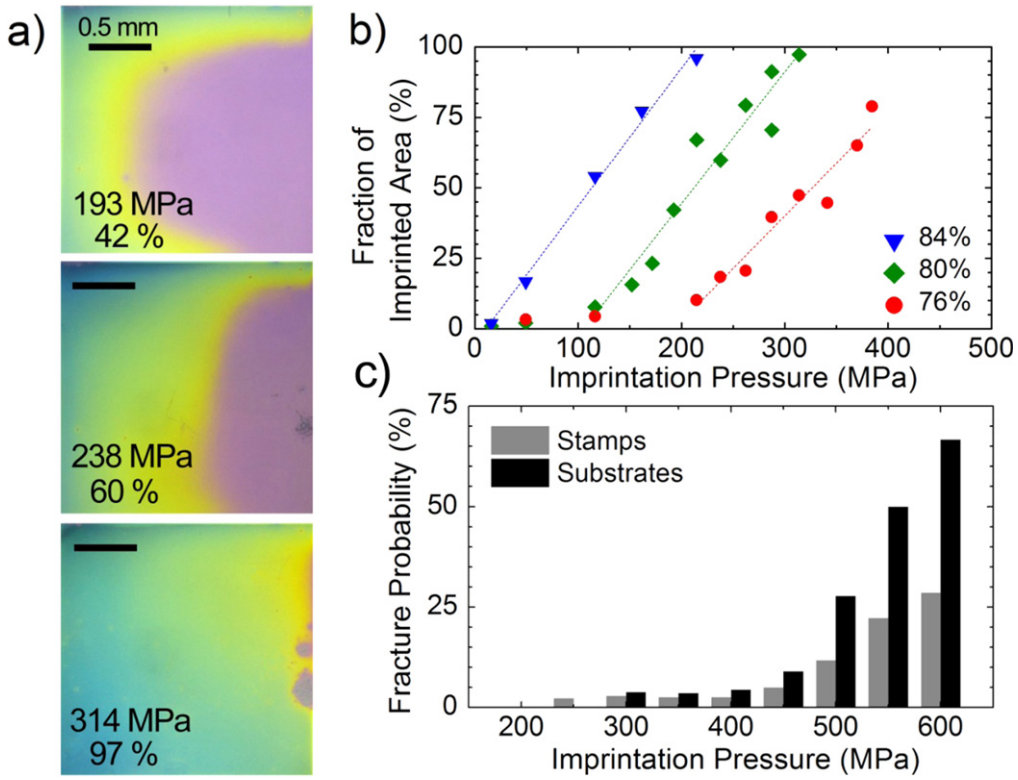

Figure 3. (a) Optical microscope images of an 80% porosity PSi film imprinted with 193, 238 and 314 MPa illustrating increased fractional imprintation with increased pressure. (b) The fractional imprintation area for PSi films of three different porosities for pressures ranging from approximately 15 MPa to the maximum pressure required for uniform pattern transfer, (c) the probability of stamp and substrate fracture for various pressures up to 600 MPa.

3. Results and discussion

Figures 1(b)–(d) show examples of PSi nanoparticles fabricated with different geometries, including ellipses, high aspect ratio rods or rectangular particles, and 'Y'-shaped, three-prong particles. The minimum achievable dimension of an imprinted PSP is approximately 100 nm, which corresponds to about 5–10 pores. Figures 1(b) and 2(b) show particles affixed to the substrate following imprinting. Figure 2(c) shows that, under optimized conditions, the interstitial, imprinted regions remain attached to the substrate following the perforation layer etch and ultrasonication. Figures 1(c) and (d) show particles following detachment from the substrate, with figure 1(d) showing a highly concentrated particle sample taken from a large quantity (>1 μg). Large batches of particles are generally monodisperse, with relatively minimal debris, as seen in figure 1(d). Minimizing the presence of irregularly-shaped debris is dependent on the carefully optimized and controlled fabrication conditions presented here.

Figure 3(b) illustrates the results of the study of imprintation area as a function of pressure for PSi films of equal thickness (250 nm), etched using 50, 60 and 70 mA cm^{-2} current densities, corresponding to approximately 76, 80 and 84% film porosities, respectively. As expected, there is a direct relationship between fraction of imprinted area and applied pressure for each etch condition. There is also an inverse relationship between the pressure required to pattern films and the porosity of the film. The curves in figure 3(b) appear to be approximately linear above some threshold that likely corresponds to the pressure below which any deformation of the PSi film is elastic. The pressures required for uniform (i.e., approximately 100%) imprintation are 215, 314 and 385 MPa for the 84, 80 and 76% porosity films, respectively. The pressures required for uniform imprintation generally agree with those reported by Ryckman *et al* [31], and also corroborates the low compressive yield strengths of PSi measured elsewhere [43]. It should be noted that no value of exactly 100% is reported in this data set due to minute imperfections in the stamp surface that are acquired over many imprintation cycles due to surface contamination, as discussed below, which preclude 'perfect' imprintation.

The longevity and mechanical robustness of the Si stamp and PSi substrates are also critical factors for fabrication throughput. For the DIPS process to be a practical approach to shape-engineered nanoparticle fabrication, stamps must be reused enough times to justify the opportunity cost of utilizing EBL for stamp fabrication. Compared to direct EBL fabrication, each imprintation of a stamp beyond the first represents a time savings approximately equal to the EBL write time, and therefore translates to a proportional cost savings in nanoparticle fabrication. In order to quantify stamp longevity, we present statistics on stamp and substrate fracture pressures (i.e., pressure of spontaneous mechanical failure) recorded over 800 imprintations, carried out with a wide variety of

imprintation conditions, to better quantify the difference in efficiency between imprinting and direct writing. The breakage probability (i.e., the number of substrate or stamp fractures that occur at a given pressure divided by the total number of imprintations carried out at that pressure) for substrates and stamps are shown in figure 3(c). In general, substrate fractures are more prevalent than stamp breakages. We hypothesize that this is due to the larger size of the substrates compared to the stamp (figure 2(a)), which results in a bending stress in the substrate during compression. At 300 MPa, a pressure commonly used to imprint PSi films of 80% porosity, the probability of substrate fracture is 3.8%, indicating that, on average, 26 imprintations may be carried out before a substrate fracture is expected. At the same pressure, the probability of stamp fracture is 2.8%, indicating that 36 imprintations can be carried out before a stamp fracture occurs. For pressures less than ~200 MPa, which are suitable for imprintation of 84% porosity films, no fractures of either stamps or substrates were recorded. It is important to note that these values do not represent absolute limitations of the process, as this data is system-specific and the method is subject to further refinement. Because the compressive yield strength of solid, non-porous Si is approximately 7 GPa, it is expected that fracture probability may be greatly reduced compared with the values presented here [27]. Indeed, multiple stamps have survived more than 150 imprintations and maintained pattern integrity. A typical stamp used in this process can yield approximately 250 ng of PSPs per imprintation (as verified by ICP-OES). Carrying out 150 imprintations therefore yields 37.5 μg of shape-engineered particles, which is a sufficient mass for *in vitro* investigations, and this can be performed in 3–5 h. In contrast, direct EBL patterning would require approximately 400 h to pattern a region of comparable size.

The DIPS process for particle fabrication could be further improved by addressing the causes of stamp deterioration and fracture. In our observation, three critical factors in the process contribute to stamp attrition: (1) roughness of the press plates utilized to compress the stamp-PSi configuration, (2) mechanical imperfections in the stamp, particularly at its edges, which act as fracture nucleation sites [45], and (3) surface contamination such as dust and Si debris that become indelibly compressed into the stamp. The first two elements are of the greatest importance in acute stamp failure, including cracking and fragmenting. The imprintation pressures applied are sufficiently high to deform hardened steel gradually over the course of 75–100 imprintations. With deformation of the plates' surfaces, stamps and substrates are subject to non-uniform compressions, increasing fracture probability. This is readily addressed, however, by regular re-surfacing of the plates. Alternatively, press plates could be formed from harder materials, such as high-strength ceramics, which could potentially eliminate imprintation-induced plate deformation. The second source of stamp failure is the number and size of defects in the stamp itself. It is well known that the stress at which brittle materials such as Si fracture is inversely proportional to the size of the defects or cracks present in the material [45]. Whether the stamp is singulated by hand-scribing, or by mechanical grinding and polishing, there are defects present that are visible with low-magnification microscopy. With automated stamp singulation, or improved polishing conditions, the size and number of defects present at stamp edges can also be significantly improved. Finally, the third source of stamp attrition, surface contamination, contributes to gradual deterioration of pattern integrity. Employing this process in a cleanroom environment (which was not the case for the work presented here) would greatly improve this element of the process. It is important to note that deterioration of stamp features due simply to pattern transfer to PSi under compression *does not* appear to lead to degradation over any number of imprintations examined thus far. The hardness of the bulk Si stamp relative to that of the high-porosity PSi is sufficiently high to prevent such deterioration [8].

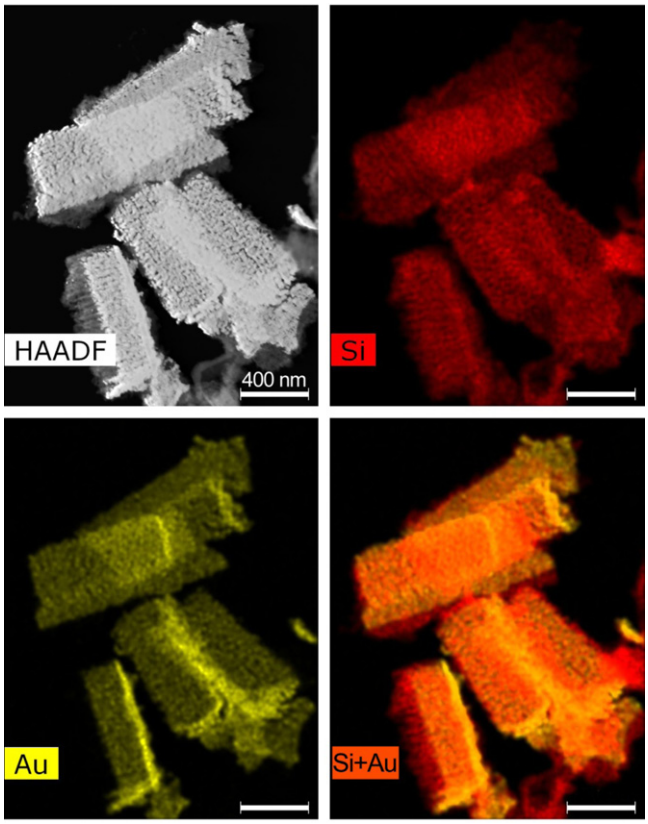

Figure 4. TEM and elemental maps of DIPS-fabricated PSi nanoparticles, functionalized with 25 nm of Au for potential use in photothermal theranostic applications.

Finally, we demonstrate that the DIPS method of particle fabrication is extensible to various methods of particle functionalization. First, because the patterning and processing is carried out on-chip, physical and chemical vapor deposition techniques may be used to produce multi-functional nano- and microparticles. Additionally, solution-based methods of drug molecule attachment can be used to load the DIPS-fabricated particles with therapeutic agents after their detachment from the Si substrate. Figure 4 shows a TEM image of a cluster of five Au-functionalized PSi nanoparticles (aspect ratio = 3.5), along with elemental EDS maps showing

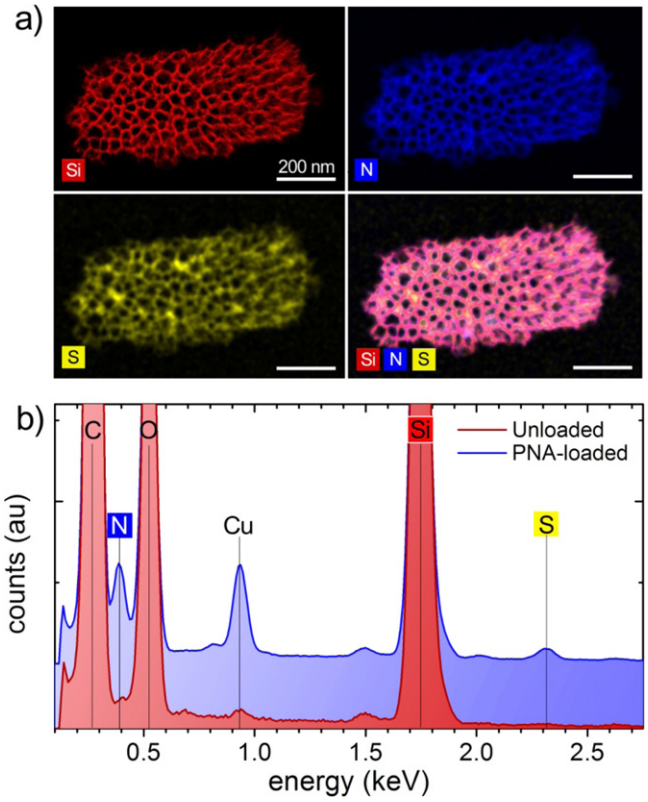

Figure 5. (a) Elemental maps of a PNA-loaded DIPS-fabricated PSi nanoparticle illustrating the distributions of Si, N and S in the drug-loaded particle, and (b) an EDS spectrum of the PNA-loaded particle as compared to a PSi control sample that is not loaded with PNA. The distinct N and S peaks indicate the presence of PNA and the linking molecule, SPDP. The Cu peak is attributed to the copper TEM grid to which the PSPs adhere.

Si and Au distributions in the particles. The image indicates uniform coating of particles on only one side (most visible in the lower left particle in figure 4), leaving the opposite side of the structure open for drug loading or other types of functionalization. Figure 5(a) shows an analogous image of elemental maps for the PNA-loaded DIPS nanoparticles. In that image, the distributions of nitrogen present in PNA and sulfur (a constituent of the SPDP linker molecule) are used to map the distribution of the drug molecules. Figure 5(b) shows a measured EDS spectrum of a PNA-loaded molecule compared to that of a control sample comprised of DIPS-patterned PSPs with no PNA present, indicating the absence of sulfur and nitrogen signatures in the control sample. Intriguingly, the elemental composite image in figure 5(a) (lower right) indicates that, while a few of the pores are visibly occluded, most of the pores remain open, which is important for allowing possible subsequent particle coating with stabilizing agents such as hydrophilic polymers.

4. Conclusions

We have presented a nanoimprintation process, DIPS, as a method to fabricate shape-engineered, multifunctional PSi micro- and nanoparticles in relatively large quantities (> tens of μg), as required for biomedical investigations. By quantifying the precise imprintation pressures required for pattern transfer, and by employing an optimized perforation layer and ultrasonic removal process, we show that stamp lifetime can be increased to more than 150 iterations of imprinting, and unwanted PSi debris incurred during fabrication can be minimized. With this stamp lifetime, approximately 40 μg of shape-engineered PSi nanoparticles can be fabricated with a single stamp in only a few (3–5) hours of imprintation. Also presented here are approaches that may be taken to further reduce stamp or substrate fracture probability and improve particle uniformity. Using this method we show that particles can be loaded with a model PNA therapeutic molecule and functionalized for more sophisticated therapeutic applications by utilizing simple material deposition techniques.

Acknowledgments

The authors thank D DeLapp for assistance in equipping the hydraulic press for PSi imprintation and R DeLapp for carrying out ICP-OES measurements. This work was supported in part by the National Science Foundation (DMR1207019). JSF and KRB acknowledge support from National Science Foundation Graduate Research fellowships.

References

[1] Alexis F, Pridgen E, Molnar L K and Farokhzad O C 2008 Factors affecting the clearance and biodistribution of polymeric nanoparticles *Mol. Pharmaceut.* **5** 505–15
[2] Anglin E J, Cheng L, Freeman W R and Sailor M J 2008 Porous silicon in drug delivery devices and materials *Adv. Drug Deliv. Rev.* **60** 1266–77
[3] Anglin E J, Schwartz M P, Ng V P, Perelman L A and Sailor M J 2004 Engineering the chemistry and nanostructure of porous silicon Fabry–Perot films for loading and release of a steroid *Langmuir* **20** 11264–9
[4] Bakry R, Vallant R M, Najam-Ul-Haq M, Rainer M, Szabo Z, Huck C W and Bonn G K 2007 Medicinal applications of fullerenes *Int. J. Nanomed.* **2** 639–49
[5] Beavers K R, Mares J W, Swartz C M, Zhao Y, Weiss S M and Duvall C L 2014 *In situ* synthesis of peptide nucleic acids in porous silicon for drug delivery and biosensing *Bioconjugate Chem.* **25** 1192–7
[6] Canham L 1997 *Properties of Porous Silicon* (London: IEE, Inspec)
[7] Canham L 2000 Porous silicon as a therapeutic biomaterial *1st Annual Int. Conf. on Microtechnologies in Medicine and Biology (Lyon)* pp 109–12
[8] Canham L 2014 *Handbook of Porous Silicon* (Berlin: Springer)
[9] Champion J A, Katare Y K and Mitragotri S 2007 Making polymeric micro- and nanoparticles of complex shapes *Proc. Natl Acad. Sci.* **104** 11901–4
[10] Chiappini C, Tasciott E, Serda R E, Brousseau L, Liu X and Ferrari M 2011 Mesoporous silicon particles as intravascular drug delivery vectors: fabrication, *in vitro*, and *in vivo* assessments *Phys. Status Solidi* C **8** 1826–32
[11] Cullis A G, Canham L T and Calcott P D J 1997 The structural and luminescence properties of porous silicon *J. Appl. Phys.* **82** 909–65

[12] Davda J and Labhasetwar V 2002 Characterization of nanoparticle uptake by endothelial cells *Int. J. Pharm.* **233** 51–9
[13] Decuzzi P, Godin B, Tanaka T, Lee S Y, Chiappini C, Liu X and Ferrari M 2010 Size and shape effects in the biodistribution of intravascularly injected particles *J. Control. Release* **141** 320–7
[14] Glangchai L C, Caldorera-Moore M, Shi L and Roy K 2008 Nanoimprint lithography based fabrication of shape-specific enzymatically-triggered smart nanoparticles *J. Control. Release* **125** 263–72
[15] Godin B, Chiappini C, Srinivasan S, Alexander J F, Yokoi K, Ferrari M, Decuzzi P and Liu X 2012 Discoidal porous silicon particles: fabrication and biodistribution in breast cancer bearing mice *Adv. Funct. Mater.* **22** 4225–35
[16] Gratton S E A, Ropp P A, Pohlhaus P D, Luft J C, Madden V J, Napier M E and DeSimone J M 2008 The effect of particle design on cellular internalization pathways *Proc. Natl Acad. Sci.* **105** 11613–8
[17] Huang X, Teng X, Chen D, Tang F and He J 2010 The effect of the shape of mesoporous silica nanoparticles on cellular uptake and cell function *Biomaterials* **31** 438–48
[18] Jiao Y, Ryckman J D, Ciesielski P N, Escobar C A, Jennings G K and Weiss S M 2011 Patterned nanoporous gold as an effective SERS template *Nanotechnology* **22** 295302
[19] Jopling C L, Yi M, Lancaster A M, Lemon S M and Sarnow P 2005 Modulation of hepatitis C virus RNA abundance by a liver-specific microRNA *Science* **309** 1577–81
[20] Korotcenkov G and Cho B K 2010 Silicon porosification: state of the art *Crit. Rev. Solid State Mater. Sci.* **35** 153–260
[21] Lawrie J L and Weiss S M 2010 Stabilization of hydroxyl-terminated silanes in porous silicon for *in situ* DNA synthesis *Phys. Status Solidi* C **8** 1851–5
[22] Lee S-Y, Ferrari M and Decuzzi P 2009 Design of bio-mimetic particles with enhanced vascular interaction *J. Biomech.* **42** 1885–90
[23] Meng H *et al* 2011 Aspect ratio determines the quantity of mesoporous silica nanoparticle uptake by a small gtpase-dependent macropinocytosis mechanism *ACS Nano* **5** 4434–47
[24] Mengistu T Z, DeSouza L and Morin S 2005 Functionalized porous silicon surfaces as MALDI-MS substrates for protein identification studies *Chem. Commun.* 5659–61
[25] Park J-H, Gu L, von Maltzahn G, Ruoslahti E, Bhatia S N and Sailor M J 2009 Biodegradable luminescent porous silicon nanoparticles for *in vivo* applications *Nat. Mater.* **8** 331–6
[26] Perry J L, Herlihy K P, Napier M E and DeSimone J M 2011 PRINT: a novel platform toward shape and size specific nanoparticle theranostics *Acc. Chem. Res.* **44** 990–8
[27] Petersen K E 1982 Silicon as a mechanical material *Proc. IEEE* **70** 420–57
[28] Roberts A P E, Lewis A P and Jopling C L 2011 miR-122 activates hepatitis C virus translation by a specialized mechanism requiring particular RNA components *Nucleic Acids Res.* **39** 1–14
[29] Ryckman J D, Jiao Y and Weiss S M 2013 Three-dimensional patterning and morphological control of porous nanomaterials by gray-scale direct imprinting *Sci. Rep.* **3** 1502
[30] Ryckman J D, Liscidini M, Sipe J E and Weiss S M 2010 Porous silicon structures for low-cost diffraction-based biosensing *Appl. Phys. Lett.* **96** 171103
[31] Ryckman J D, Liscidini M, Sipe J E and Weiss S M 2011 Direct imprinting of porous substrates: a rapid and low-cost approach for patterning porous nanomaterials *Nano Lett.* **11** 1857–62
[32] Sahay G, Alakhova D Y and Kabanov A V 2010 Endocytosis of nanomedicines *J. Control. Release* **145** 182–95
[33] Sailor M J 2012 *Porous Silicon in Practice: Preparation, Characterization and Applications* (Weinheim: Wiley)
[34] Salonen J, Laitinen L, Kaukonen A M, Tuura J, Björkqvist M, Heikkilä T, Vähä-Heikkilä K, Hirvonen J and Lehto V P 2005 Mesoporous silicon microparticles for oral drug delivery: loading and release of five model drugs *J. Control. Release* **108** 362–74
[35] Santos H A, Riikonen J, Salonen J, Mäkilä E, Heikkilä T, Laaksonen T, Peltonen L, Lehto V-P and Hirvonen J 2010 *In vitro* cytotoxicity of porous silicon microparticles: effect of the particle concentration, surface chemistry and size *Acta Biomater.* **6** 2721–31
[36] Sau T K and Rogach A L 2010 Nonspherical noble metal nanoparticles: colloid-chemical synthesis and morphology control *Adv. Mater.* **22** 1781–804
[37] Sharma G, Valenta D T, Altman Y, Harvey S, Xie H, Mitragotri S and Smith J W 2010 Polymer particle shape independently influences binding and internalization by macrophages *J. Control. Release* **147** 408–12
[38] Smith R L and Collins S D 1992 Porous silicon formation mechanisms *J. Appl. Phys.* **71** R1–22
[39] Stewart M P and Buriak J M 2000 Chemical and biological applications of porous silicon technology *Adv. Mater.* **12** 859–69
[40] Tanaka T *et al* 2010 Sustained small interfering RNA delivery by mesoporous silicon particles *Cancer Res.* **70** 3687–96
[41] Trewyn B G, Slowing I I, Giri S, Chen H-T and Lin V S Y 2007 Synthesis and functionalization of a mesoporous silica nanoparticle based on the sol–gel process and applications in controlled release *Acc. Chem. Res.* **40** 846–53
[42] Vaccari L, Canton D, Zaffaroni N, Villa R, Tormen M and di Fabrizio E 2006 Porous silicon as drug carrier for controlled delivery of doxorubicin anticancer agent *Microelectron. Eng.* **83** 1598–601
[43] Wang F, Zhao K, Cheng J and Zhang J 2011 Conciliating surface superhydrophobicities and mechanical strength of porous silicon films *Appl. Surf. Sci.* **257** 2752–5
[44] Wu E C, Andrew J S, Cheng L, Freeman W R, Pearson L and Sailor M J 2011 Real-time monitoring of sustained drug release using the optical properties of porous silicon photonic crystal particles *Biomaterials* **32** 1957–66
[45] Yang C, Mess F, Skenes K, Melkote S and Danyluk S 2013 On the residual stress and fracture strength of crystalline silicon wafers *Appl. Phys. Lett.* **102** 021909
[46] Zauner W, Farrow N A and Haines A M R 2001 *In vitro* uptake of polystyrene microspheres: effect of particle size, cell line and cell density *J. Control. Release* **71** 39–51